

Simulation of drilling-induced compaction bands using discrete element method

Rahmati, H.¹, Nouri, A.¹, Chan, D.¹, Vaziri, H.²

Abstract

Rock failure is observed around boreholes often with certain types of failure zones formed which are called breakouts. Drilling experiments in some high porosity quartz-rich sandstone have shown that breakouts are formed by developing a narrow localized compacted zone in the minimum horizontal stress direction. They are called fracture-like breakouts.

Such compaction bands may affect hydrocarbon extraction by forming barriers that inhibit fluid flow and may also be a source of sand production. Therefore, investigation of the mechanism of fracture-like breakout has received considerable attention in the past ten years in the oil industry due to its potential impact on the performance of oil wells.

This paper presents the results of numerical simulations of borehole breakouts using three dimensional discrete element method (DEM) to investigate the mechanism of the fracture-like breakouts and to identify the role of far-field stresses on breakout dimensions. The numerical tool was first verified against analytical solutions. It was then utilized to investigate the failure mechanism and breakout geometry for drilled cubic rock samples of Castlegate sandstone subjected to different pre-existing far-field stresses to simulate the drilling experiments.

The results show that failure occurs in the zones of the highest concentration of tangential stress around the borehole in the direction parallel to the minimum horizontal stress. It is concluded that fracture-like breakout will develop as a result of non-dilatant micro-mechanism consisting of localized grain debonding and grain crushing which leads to the formation of a compaction band in the minimum horizontal stress direction. In addition, it is found that the length of fracture-like breakouts depends on both the mean stress and stress anisotropy. However the width of the breakout is not significantly changed by far-field stresses.

Introduction

The term “borehole breakout” is normally associated with borehole cross-sectional elongations resulting from preferential rock failure at and behind the borehole wall during or after drilling (Haimson and Song, 1998). Borehole breakouts in oil wells drilled in deep sandstone formations can cause wellbore instability during drilling, affecting well completion design and well operational limits (Germanovich and Dyskin, 2000).

¹ Department of Civil and Environmental Engineering, University of Alberta

² BP America Inc.

Bell and Gough (1979) first observed that breakouts in wellbores drilled in the oil fields of Alberta, Canada are aligned with the minimum in-situ horizontal stress, σ_h , and they proposed a systematic correlation between the breakout orientation and the direction of the regional horizontal stress, σ_h . Since then, several researchers have suggested a correlation between the breakout orientation and borehole dimensions, and the directions and magnitudes of the in-situ stresses through experimental findings (e.g. Haimson and Herrick, 1986; Haimson and Song, 1993; Herrick and Haimson, 1994; Haimson and Lee, 2004), based on theoretical works (e.g. Gough and Bell, 1982; Zoback et al., 1985; Zheng et al., 1989; Shen et al., 2002) and based on field observations (e.g. Barton 1988; Zoback and Magee, 1991).

Three common types of breakouts have been observed in sandstone from hollow cylinder tests (Lavrov et al., 2005). They are: (a) uniform failure round the borehole, (b) dog-ear breakouts, and (c) fracture-type breakouts, see Fig. 1.

In uniform failure around the wellbore, the deformation of the surface around the opening is uniform and the cavity remains nearly circular after failure. Fig. 1a shows the failure pattern from a X-ray CT-scan image of a hollow cylinder test sample, which shows shear bands are distributed uniformly around the cavity (Lavrov et al., 2005).

The second type of failure resembles two nearly identical V-shaped breakouts that is developed in diametrically opposite sides of the hole in the direction of the minimum horizontal principal stress (Fig. 1b). The V-shaped breakouts are attributed to either tensile spalling or shear fracturing or a combination of the two modes (Vardoulakis et al., 1988; Guenet, 1989).

Haimson and Song (1998) and Haimson (2001) found that in highly porous sandstone, fracture-like failure bands can develop in the direction of the minimum principal stress (Fig. 1c). Later Klaetch and Haimson (2002) and Haimson and Lee (2004) observed similar fracture-like failure pattern in St. Peter sandstone and Mansfield sandstone. Scanning electron microscope (SEM) images showed that fracture-like breakouts developed by the formation of a narrow band of compacted grains ahead of the breakout tip. Grains were either crushed or broken and repacked within the compacted band, leading to significant porosity reduction. Based on numerical simulations, Lavrov et al. (2005) concluded that elongated slits are associated with tensile failure at the tip of the slit in contrast to Haimson's observations.

Several attempts have been made to investigate the failure pattern around the borehole based on theoretical works, notably using elasto-plasticity (Kwong and Kaiser, 1989; Zheng et al., 1989; Papamichos et al., 2001; Detournay et al., 2009), pressure-dependent elasticity (Santarelli and Brown, 1987; Santarelli and Brown, 1989), bifurcation theory (Papanastaiou and Vardoulakis, 1992), fracture mechanics (Bazant et al., 1993; Germanovich and Dyskin, 2000) and microstatistics (Charlez et al., 1989). A comprehensive review of many theoretical and numerical approaches to investigate the mechanism of the borehole breakouts has been provided by Germanovich and Dyskin (2000).

Several researchers have identified the Discrete Element Method (DEM) as a useful tool in the investigation of breakout morphology and sand production (Rawling et al., 1993; O'Connor et al., 1997; Jensen et al., 2000; Li et al., 2006). Instead of treating the rock mass as a continuum, DEM simulates the particles/blocks and their interaction explicitly (Jing and Stephansson, 2007).

Rawling et al. (1993) investigated the influence of natural fractures, stress anisotropy and wellbore orientation on wellbore stability and breakout geometry. Their model was based on direct simulation of block movements using a DEM code called UDEC (Itasca, 2000) to investigate the mechanism of uniform and V-shaped breakouts in heavily pre-fractured rocks. Li et al. (2006) used two dimensional commercial DEM code, PFC2D (Itasca, 2004), to simulate hollow cylinder tests with fluid flow and study sanding and breakout geometry. PFC2D simulates an assembly of circular disks with the bonds inserted between them. In the standard PFC2D code, the bonds have normal and shear stiffness and strength and they fail when the tensile or shear stress in the bond exceeds its strength (Itasca, 2004). Li et al. (2006) used bond strength so high that no bonds in the model would fail due to the stress in the bond. It is assumed that all bonds associated with a given disk break when the stresses inside the disk satisfy a failure criterion. In addition, grain crushing is simulated by reducing particle radius when the particle stresses reached a threshold. They found three typical breakout geometries in the simulations similar to those observed in laboratory tests. The fracture-like breakout was observed when the material is prone to localized compressive failure. However, the compacted zone of reduced porosity was not observed at the breakout tip. For those cases where the material was weak and the tensile strength was low, uniform failure around the borehole was observed along with a rather uniform hole enlargement. In those cases with relatively competent rock properties, which were unlikely to fail in localized compaction, the failure pattern was observed to be in the form of V-shaped breakouts.

Little is known on the mechanism of the initiation and propagation of the compaction bands at the grain scale during drilling. This paper describes the development of drilling induced compaction bands using a three dimensional discrete element model to investigate the mechanism of the fracture-like breakout at the particle scale. The numerical tool was verified against analytical solution and then utilized to study the effect of stresses on the breakout length and shape in cubic laboratory rock samples.

Theoretical Background

A DEM analysis involves modeling granular materials using assembly of particles that allows inter-particle interactions. Cundall (1971) first introduced the DEM in the analysis of rock blocks failure. A comprehensive description of the DEM is given by Potyondy and Cundall (2004).

The particle flow code (PFC3D) developed by Itasca was used in the three dimensional DEM simulations of well hole failure presented here. PFC3D is based on Cundall and Strack's (1979) work which is a simplified implementation of the DEM. In PFC3D, the particles are assumed to

be rigid but small overlaps are allowed at the contact points (Itasca, 2008). These overlaps mimic the deformations that occur in real particle contacts of geomaterials. The parallel bond model in PFC3D is considered to be an appropriate bonding model for DEM models of cemented sands (Potyondy and Cundall, 2004). The parallel bond models are able to transmit both forces and moments, like the cementing materials do at real contacts.

In this work, a numerical scheme was implemented in PFC3D to simulate grain crushing during the formation of the compaction bands that are believed to induce fracture-like breakouts.

The Grain Crushing Modeling Scheme

In addition to the tensile and shear failure at inter-granular contacts that are captured in the standard PFC3D, the model used in this research includes a scheme to simulate grain breakage and crushing.

Several researchers have proposed a number of schemes to model grain breakage in DEM simulations (Tsoungui et al., 1999; Couroyer et al., 2000; Cheng et al., 2003; Marketos and Bolton, 2009). The schemes use some simplifying assumptions to capture the behaviour without dramatically increasing simulation time.

The breakage criterion is usually defined in terms of contact forces acting on the grain (Couroyer et al., 2000; Marketos and Bolton, 2009). In this research, a particle will break if the characteristic stress (σ_{ch}) inside the particle exceeds its crushing strength (σ_{crush}) (Marketos and Bolton, 2009):

$$\sigma_{ch} = \frac{F_{(max)particle}}{D^2} \geq \sigma_{crush}, \text{ grain breaks}$$

The characteristic stress (σ_{ch}) is defined as the ratio of the maximum normal contact force ($F_{(max)particle}$) on the particle to the square of its diameter (D). The crushing strength (σ_{crush}) has been experimentally evaluated by conducting single grain crushing tests. The test is conducted by inserting a grain between two platens and then moving the lower platen to crush the grain. The crushing strength is defined as the ratio of the maximum force at failure to the square of the distance between the platens at the start of the test (Mcdowell and Amon, 2000; Nakata et al., 2001). Nakata et al. (2001) concluded that the grain crushing strength depends on the grain mineralogy and the grain size.

In the DEM simulation of the compaction band, different methods were used to simulate the post breakage behaviour. A comprehensive review of the methods is given by Marketos and Bolton (2009). One of the methods for modeling grain crushing is to reduce the contact stiffness of the crushed particle (Marketos and Bolton, 2009). The stiffness reduction simulates the deformation of inter-fragment voids making the local response less stiff. The amount of stiffness reduction depends on the grain mineralogy and the stresses on the crushed particle by the neighbouring

grains. After breakage, the broken particle could still carry force resulting in reduction in the compaction band porosity. Kurt et al. (2005) found that the elastic modulus within the compaction band increases as the result of porosity reduction and the increased area of contact among the grains.

The Numerical Modeling Case

Numerical model has been used to simulate drilling in laboratory samples of the Castlegate sandstone. The numerical procedure was designed to closely simulate the drilling conditions, in which the wellbore material is removed while the rock is under some in-situ stresses. The applied stresses were sufficiently high that generated breakouts around the hole.

Test numerical specimens were generated in a rectangular box of $0.18 \text{ m} \times 0.18 \text{ m} \times 0.02 \text{ m}$ ($W \times H \times D$) bounded by rigid frictionless walls. To ensure initial tight packing, the particles were generated at half their final size. Then the particle diameters were increased to their final values under zero friction (frictionless balls). The walls were moved slowly using a servo-control algorithm, until the block reached an isotropic stress state of 0.2 MPa. This low value of isotropic stress is around one percent of uniaxial compressive strength and it was chosen to reduce the locked-in stresses that develop after subsequent parallel-bond installation (Itasca, 2008). In order to have a denser network of parallel bonds in the subsequent step, floating particles, defined as the particles with less than three contacts with other particles, were removed (Potyondy and Cundall, 2004). Next, parallel bonds were randomly installed at 30 % of the contacts detected at this stage, and the bond radius multiplier was varied randomly between 0 and 1 based on the observations from the Scanning Electron Microscope (SEM) images for the Castlegate sandstone (Cheung, 2010). Then a friction coefficient was assigned to all particles.

The specimen consisted of 89,538 spherical particles of sizes randomly between 0.4 and 1.3 mm which approximately captures the particle size distribution of the Castlegate sandstone (Fig. 2). It is to be noted that it is not practical to model every single grain in the DEM simulations with the current computational power. Therefore, particles that represent rock volumes rather than individual grains are modeled in DEM. Other DEM micro parameters were calibrated to match the DEM response with the triaxial tests measurements on the Castlegate sandstone (Table 1). Fig. 3 compares the macro-responses of the DEM triaxial model under different confining stresses with the corresponding laboratory results.

The average porosity of the DEM specimen was assessed to be 0.34 which is more than the actual porosity (0.25). This is partly because the parallel bond representing the cement between grains is represented as a set of springs with no volume. Moreover, the particles in PFC3D are spherical whereas in the Castlegate sandstone, grains are sub-angular and usually have irregular shapes (Cheung, 2010). This could also affect the packing and therefore the initial porosity of the specimen.

In our simulations, the stiffness of a crushed particle is reduced by a factor of two once the grain-crushing criterion is satisfied (Marketos and Bolton, 2009). Alvarado (2007) reported that the Castlegate sandstone particles are predominately quartzitic. The average particle crushing strength was assumed to be 60 MPa based on the single grain crushing experiments that Nakata et al. (2001) conducted on different sizes of quartzitic grains. In addition, it was assumed that the contact stiffness after grain crushing increases linearly as a function of porosity to eventually reach the original contact stiffness.

The simulation procedure started by applying three perpendicular and unequal stresses ($\sigma_H \geq \sigma_V \geq \sigma_h$) using a servo control algorithm. While maintaining the far-field stresses on the specimen, a vertical borehole (1.25 cm radius) was drilled by gradually decreasing the grains stiffness inside the borehole to zero and finally removing the grains from inside the hole. Then the model was cycled till the average unbalanced forces were low compared to the average contact forces (0.01 ratio was adopted here).

Verification of the DEM model- The DEM simulations were verified by comparing their response with the calculated results from analytical solutions. Zoback (2007) derived analytical expressions for the effective stresses at the wellbore wall in an anisotropic elastic medium.

In the analytical solution and DEM model, the maximum horizontal, vertical and minimum horizontal stresses were 40, 30 and 20 MPa respectively. The applied stresses were selected such that the material response at the borehole wall was elastic. The sample was also assumed to be dry. Fig. 4 compares the stresses in a cylindrical coordinate system at the wellbore wall of the DEM model with the analytical solution in terms of the angle with respect to the direction of the maximum horizontal stress. It shows that the radial stress is zero at the wellbore wall and the tangential and vertical stresses vary as a function of position around the wellbore, in which they are strongly compressive in the direction of the minimum horizontal stresses. Note that the average value of vertical stress is the same as the far-field vertical stress (30 MPa) and the variation of the tangential stress is around four times of the difference between the maximum and minimum horizontal stresses ($4 \times (40 - 20) = 80$ MPa).

In addition, the DEM simulations were also verified by comparing the DEM response with the calculated results from analytical solutions developed by Risnes et al. (1982). They derived analytical expressions for the stresses around a wellbore or cavity using continuum based elasticity and plasticity theories. They assumed axisymmetry and plane strain conditions and that the material obeys the Mohr-Coulomb failure criterion.

In the analytical model, a disk of Castlegate sandstone with an inner radius (R_i) of 8 mm, outer radius of 80 mm and unit height was chosen. The sample was also assumed to be dry. The other input parameters for the analytical solution, including cohesion, friction angle and Poisson's ratio were assumed to be equal to 4.3 MPa, 46.5° and 0.2, respectively. The cohesion and friction angle were evaluated at peak strength from the simulated triaxial tests on the Castlegate

sandstone assuming the material obeys Mohr-Coulomb model. Young's modulus was determined at 50% of the peak stress (Jafarpour et al., 2012). Also, the average Poisson's ratio at different effective confining stresses was used in the calculations.

Fig. 5 shows the analytical vertical and tangential stress profiles. The extent of the plastic zone is shown by R_c where the peak tangential stress is observed.

The DEM model was generated by three rigid walls (two horizontal and one cylindrical) with a radius of 80 mm and height of 15 mm. The micro-parameters were the same as the parameters in the calibration for Castlegate sandstone. A radial stress of 50 MPa was applied to the cylindrical wall using a servo control algorithm while the top and the base platen remained stationary. Then the inner hole was drilled by removing the particles and the model was cycled till the average unbalanced forces were low compared to the average contact forces (0.01 ratio was adopted here).

Fig. 5 compares the stresses around the wellbore of the DEM model with the analytical solution. The stress in the DEM model was calculated by performing a statistical averaging technique over a representative volume based on the algorithm described in Potyondy and Cundall (2004). The radial stress gradually increased from zero at the well face to 50 MPa at the outer boundary, and the tangential stress increased and reached a maximum value in the plastic zone and then decreased in the elastic zone. The stress values and the size of the plastic zone are in agreement with the analytical solutions.

Numerical results

The borehole breakout simulations were performed at the maximum horizontal stress ($\sigma_H = 50$ MPa), the vertical stress ($\sigma_v = 30$ MPa) and the minimum horizontal stress ($\sigma_h = 20$ MPa) on the solid Castlegate sandstone sample.

The results of the simulations are presented in Figs. 6 and 7. Fig. 6 shows a horizontal cross section of the sample after completion of drilling. Micro-scale damage at the contacts is presented by red lines for bonds failed in tension and the blue lines for the bonds failed in shear. The yellow grains show intact grains while the black ones represent the crushed grains. Fig. 6 shows the induced breakout is aligned with the minimum horizontal stress direction where the stress concentration is the highest. Breakout is initiated at the borehole wall by grain debonding and progressed with additional grain debonding and grain crushing resulting in the formation of a compaction band in the direction of σ_h or the springline of the opening. This breakout resembles fracture-like breakout observed in Castlegate sandstone (Cundall et al., 1999) and a high-porosity sandstones (Haimson, 2007) in the laboratory drilling experiments.

By the time the breakout is fully developed, the total number of broken bonds is only 310 while 1,484 particles are crushed inside the compaction band. The average porosity along the compaction band after drilling is 0.325 which is less than the initial porosity (0.34). Thus it

shows that the failure mechanism is not of a dilatant nature as in V-shaped breakouts (Haimson, 2007). Also, the length of the reduced porosity zone from the borehole center (L) was 4.3 cm.

The density of the broken bonds is defined as the total number of broken bonds (which fail in either tension or shear) within the unit length of the compaction band in the entire height of the specimen. Fig. 7 shows that the density decreases with distance from the face of the wellbore within the compaction band. More bonds are broken near the face of the wellbore and therefore it could facilitate particle removal by seepage forces if there is fluid flow.

Haimson and Lee (2004) experimentally showed that fracture-like breakout dimensions in Mansfield sandstone depend on the far-field stresses. In this research, the effect of far-field stresses on breakout dimensions was examined using the DEM on Castlegate sandstone. The simulations were conducted at different levels of the minimum and maximum horizontal stress (σ_h and σ_H) and vertical stress (σ_v). The results show fracture-like breakout in the σ_h direction (Fig. 8).

Fig. 9 shows the breakout length (normalized using the hole radius) as a function of the ratio between the maximum and minimum horizontal stresses (σ_H/σ_h). It shows that the slit length increases with increasing σ_H at constant σ_h (increasing σ_H/σ_h), which is in agreement with Haimson and Lee (2004). However, the length decreases at constant (σ_H) with decreasing σ_h (increasing σ_H/σ_h), which results in lower mean stress (e.g., comparing points A and B in Fig. 9). This suggests that both mean stress and stress anisotropy can affect the fracture-like breakout dimension. Thus, the slit length alone cannot be used as an indicator of the magnitudes of the far-field horizontal stress. This phenomenon could be explained by the failure mechanism of the fracture-like breakout.

As mentioned above, compaction band forms as a result of grain debonding and grain crushing. Fig. 10a illustrates that more bonds break with increasing the stress anisotropy ($\sigma_H-\sigma_h$) and Fig. 10b shows that more grains crush with increasing the mean stress. Thus, in addition to the σ_H/σ_h ratio (which results in grain debonding), the mean stress (which results in grain crushing) plays an important role in fracture-like breakout dimensions. This could also be the reason that less stress anisotropy (less σ_H/σ_h) is needed to initiate fracture-like breakout at higher minimum horizontal and vertical stresses, therefore higher mean stress (by extrapolating the lines in Fig. 9 to $L/r=1$).

The average width of the fracture-like breakout was measured at different far-field stresses (Fig. 8). It is found that the average width remained almost constant ($7 \text{ mm} \pm 2 \text{ mm}$) regardless of the magnitudes of the far-field stresses. Haimson and Kavocich (2003) experimentally showed similar behaviour in fracture-like breakout in Berea sandstone.

Conclusions

A three dimensional numerical model has been developed to investigate fracture-like breakout around wellbore due to drilling. The model is based on discrete element method and improved by implementing a grain-crushing algorithm to investigate the fracture-like breakout mechanism at the microscopic particle scale. The numerical tool was also verified against analytical solutions.

The DEM model was used to simulate drilling in the Castlegate sandstone in which the applied stresses were sufficiently high that generated breakout around the hole. The results show that fracture-like breakout develops as a result of formation of compaction bands and possible grain crushing in the direction of σ_h . Contrary to V-shaped breakout, the failure mechanism in fracture-like breakout is non-dilatant and the failure zone has a lower porosity than before and a compaction band is formed along with the σ_h springline.

Stress analysis was conducted to explore the relation between far-field stresses and the size of the fracture-like breakout. It is found that the slit-facture length depends on both the mean stresses and the extent of stress anisotropy. Therefore the slit-facture length alone cannot be used to determine far-field stresses. It is also found that the width of the fracture-like breakout does not significantly change with changing far-field stresses.

Acknowledgements

The authors would like to acknowledge the research funding for this study provided by NSERC through their Discovery Grants Program. We also thank BP for their technical advice, providing and permitting the publication of the laboratory data.

References

1. Barton, C.A., 1988. Development of in situ stress measurement techniques for deep drillholes. PhD Dissertation, Stanford University, Palo Alto.
2. Bazant, Z.P., Lin, F.B., Lippman, H., 1993. Fracture energy release and size effect in borehole breakout. *Int. J. Num. Anal. Meth. Geomech.*, Vol. 17, No. 1, pp. 1-14.
3. Bell, J.S., Gough, D.I., 1979. Northeast-southwest compressive stress in Alberta: Evidence from oil wells. *Earth and Planetary Science Letters*, Vol. 45, No. 2, pp. 475-482.
4. Charlez, P.H., Segal, A, Heugas, O., Quenault, O., Chevreuse, S.T.R., 1989. Development of a microstatistical model for deep borehole ovalization in brittle rocks. *ISRM International Symposium, Pau, France, Aug. 30 – Sep. 2.*
5. Cheng, Y.P., Nakata, Y., Bolton, M.D., 2003. Discrete element simulation of crushable soil. *Geotechnique*, Vol. 53, No. 7, pp. 633–641.
6. Cheung, L.Y.G., 2010. *Micromechanics of Sand Production in Oil Wells*, PhD Thesis, Imperial College of London, London.

7. Couroyer, C., Ning, Z., Ghadiri, M., 2000. Distinct element analysis of bulk crushing: effect of particle properties and loading rate. *Powder Technology*, Vol. 109, No. 1-3, pp. 241–254.
8. Cundall, P.A., Damjanac, B., Pestman, B.J., 1999. Compression cracks observed in numerical simulations of a thick wall cylinder in porous sandstone. *EOS Trans AGU, Union* 80:F1068.
9. Cundall, P.A., 1971. A computer model for simulating progressive large scale movement in blocky rock systems. *Proceeding Symposium in international society of rock mechanics*, Nancy, France.
10. Cundall, P.A., Strack, O.D.L., 1979. A discrete numerical model for granular assemblies. *Geotechnique*, Vol. 29, No.1, pp. 47-65.
11. Detournay, C., 2009. Numerical modelling of the slit mode of cavity evolution associated with sand production. *SPEJ*, Vol. 14, No. 4, pp. 797-804.
12. Germanovich, L.N., Dyskin, A.V., 2000. Fracture mechanisms and instability of openings in compression, *International Journal of Rock Mechanics and Mining Sciences*, Vol. 37, No. 1-2, pp. 263-284.
13. Gough, D.I., Bell, J.S., 1982. Stress orientations from borehole wall fractures with examples from Colorado, east Texas, and Northern Canada. *Can. J. of Earth Sci.*, Vol. 19, No. 7, pp. 1358-1370.
14. Guenot, A., 1989. Borehole breakouts and stress fields. *International Journal of Rock Mechanics and Mining Sciences and Geomechanics*, Vol. 26, No. 3, pp 185-195.
15. Haimson, B.C., 2001. Fracture-like borehole breakouts in high-porosity sandstone: Are they caused by compaction bands. *Physics and Chemistry of the Earth Part A Solid Earth and Geodesy*, Vol. 26, No. 1-2, pp. 15-20.
16. Haimson, B., Lee, H., 2004. Borehole breakouts and compaction bands in two high-porosity sandstones. *Int. J. Rock Mech. Min. Sci.*, Vol. 41, pp. 287-301.
17. Haimson, B., 2007. Micromechanisms of borehole instability leading to breakouts in rocks, *Int. J. Rock. Mech. Min. Sci.*, Vol. 44, pp. 157-173.
18. Haimson, B., Kovacich, J., 2003. Borehole instability in high-porosity Berea sandstone and factors affecting dimensions and shape of fracture-like breakouts. *Engineering Geology*, Vol. 69, No. 3-4, pp. 219-231.
19. Haimson BC, Song I., 1998. Borehole breakouts in Berea sandstone: two porosity-dependent distinct shapes and mechanism of formation. *Rock Mechanics in Petroleum Engineering*, Trondheim, Norway, July 8-10.
20. Haimson, B.C., Herrick, C.G., 1986. Borehole breakouts – a new tool for estimating in situ stress? *Proc. Int. Symp. on Rock Stress and Rock Stress Meas.*, Stockholm, Publ. Lulea, Centek, pp. 271-280.
21. Haimson, B.C., Song, I., 1993. Laboratory study of borehole breakouts in Cordova Cream: a case of shear failure mechanism. *Int. J. Rock Mech. Min. Sci. Geomech. Abstr.*, Vol. 30, No. 7, pp. 1047-1056.

22. Herrick, C.G., Haimson, B.C., 1994. Modeling of episodic failure leading to borehole breakouts in Alabama limestone. Proc. of the First North American Rock Mechanics Symp., Austin, Balkema, Rotterdam, eds. P. Nelson and S. Laubach, pp. 217-224.
23. Itasca Consulting Group, Inc. PFC3D, Version 4.0. Minneapolis: Itasca, 2008.
24. Itasca Consulting Group, Inc. PFC2D, Version 4.0. Minneapolis: Itasca, 2004.
25. Itasca Consulting Group, Inc. UDEC, Minneapolis: Itasca, 2000.
26. Jafarpour, M., Rahmati, H., Azadbakht, S., Nouri, A., Chan, D., Vaziri, H., (in press). Determination of Mobilized Strength Properties of Degrading Sandstone. Journal of Soils And Foundations.
27. Jensen, R.P., Preece, D.S., 2000. Modeling of sand production with Darcy's flow coupled with discrete element. OSTI.
28. Jing, L., Stephansson, O., edition 2007. Fundamentals of discrete element methods for rock engineering, theory and applications. Elsevier.
29. Klaetch, A.R., Haimson, B.C., 2002. Porosity-dependent fracture-like breakouts in St. Peter sandstone. Hammah R, et al., editor. Mining and tunneling innovation and opportunity. University of Toronto Press, Toronto, pp. 1365-71.
30. Kurt, R.S., Rudnicki, J.W., Pollard, D.D., 2005. Anticrack inclusion model for compaction bands in sandstone. Journal of Geophysical Research, Vol. 110.
31. Kwong, A, Kaiser, P.K., 1989. Stability of tunnels in rock with localized weaknesses. In: Lo E, editor. Proceedings of the International Congress on Progress Innovation in Tunnelling, vol. 1, pp. 341-358.
32. Lavrov, A., Cerasi, P., Papamichos E., 2005. Numerical modeling of sand production mechanisms with displacement discontinuity method. SPE Europec/EAGE Annual Conference, Madrid, Spain, June 13-16.
33. Li, L., Papamichos, E., Cerasi, P., 2006. Investigation of sand production mechanisms using DEM with fluid flow, Multiphysics Coupling and Long Term Behaviour in Rock Mechanics ISRM Eurock 2006, Liège, Belgium, pp. 241-247.
34. Marketos, G., Bolton, M.D., 2009. Compaction bands simulated in discrete element models. Journal of Structural Geology, Vol. 31, pp. 479-490.
35. McDowell, G.R., Amon, A., 2000. The application of Weibull statistics to the fracture of soil particles. Soils and Foundations, Vol. 40, No. 5, pp. 133-141.
36. Nakata, Y., Kato, Y., Hyodo, M., Hyde, A.F.L., Murata, H., 2001. One-dimensional compression behaviour of uniformly graded sand related to single particle crushing strength. Soils and Foundations, Vol. 41, No. 2, pp. 39-51.
37. O'Connor, M., Torczynski, J.R., Preece, D.S., Klosek, J.T., Williams, J.R., 1997. Discrete element modeling of sand production, International Journal of Rock Mechanics and Mining Sciences, Vol. 34, No. 3-4, pp. 231.e1-231.e15.

38. Papamichos, E., Vardoulakis, I., Tronvoll, J., Skjaerstein, A., 2001. Volumetric sand production model and experiment. *International Journal for Numerical and Analytical Methods in Geomechanics*, Vol. 25, pp. 789-808.
39. Papanastasiou, P., Vardoulakis, I., 1992. Numerical treatment of progressive localization in relation to borehole stability. *Int. J. Num. Meth. Geomech.*, Vol. 16, pp. 389-424.
40. Potyondy, D.O., Cundall, P.A., 2004. A bonded particle model for rock. *International Journal of Rock Mechanics & Mining Sciences*, Vol.41, No.8, pp. 1329-1364.
41. Rawling, N.R., Barton, S.C., Bandis, S.C., Addis, M.A., Gutierrez, M.S., 1993. Laboratory and numerical discontinuum modeling of wellbore stability. *JPT*, Vol. 45, No. 11, pp. 1086-1092.
42. Risnes R., Bratli R, Horsrud, P., 1982. Sand stresses around a wellbore. *Society of Petroleum Engineers Journal*, Vol. 22, No. 6, pp. 883-898.
43. Santarelli, F.J., Brown, E.T., 1987. Performance of deep wellbores in rock with a confining pressure-dependent elastic modulus. *Proc. 6th ISRM Congr., Montreal, Canada*, Aug. 30- Sep. 3.
44. Santarelli, F.J., Brown, E.T., 1989. Failure of three sedimentary rocks in triaxial and hollow cylinder compression tests. *Int. J. Rock Mech. Min. Sci. & Geomech. Abstr.*, Vol. 26, pp. 401-413.
45. Shen, B., Stephansson, O., Rinne, M., 2002. Simulation of borehole breakouts using FRACOD2D. *Oil & Gas Science and Technology – Rev. IFP*, Vol. 57, No. 5, pp. 579-590.
46. Tsoungui, O., Vallet, D., Charmet, J.C., 1999. Numerical model of crushing of grains inside two-dimensional granular materials. *Powder Technology*, Vol. 105, No. 1-3, pp. 190–198.
47. Vardoulakis, I., Sulem, J., Guenot, A., 1988, Borehole instabilities as bifurcation phenomena. *Int. J. Rock. Mech. Min. Sci. & Geomech. Abstr.*, Vol. 25, No. 3, pp. 159-170.
48. Zheng, Z., Kemeny, J., Cook, N.G.W., 1989. Analysis of borehole breakouts. *Journal of Geophysical Research*, VOL. 94, NO. B6, PP. 7171-7182.
49. Zoback, M.D., Moos, D., Mastin, L., Anderson, R.N., 1985. Wellbore breakouts and in situ stress. *Journal of Geophysical Research*, Vol. 90, No. B7, pp. 5523-5530.
50. Zoback, M., Magee, M., 1991. Stress Magnitudes in the Crust: Constraints from Stress Orientation and Relative Magnitude Data. *Phil. Trans. R. Soc. Lond. A*, Vol. 337, No. 1645, pp. 181-194
51. Zoback, M., 2007. *Reservoir geomechanics*. Cambridge University Press.

Tables

Table 1. Calibrated micro-parameters for the Castlegate sandstone DEM model

Particle properties		Parallel bond properties	
Particle contact modulus, E (GPa)	7	Cement Young's modulus, E_{pb} (GPa)	20
The ratio of normal to shear stiffness of the particles, $\frac{K^N}{K^S}$	0.2	The ratio of normal to shear stiffness of the cement, $\frac{K_{pb}^N}{K_{pb}^S}$	0.2
The particle friction coefficient, μ	1.5	Normal strength of the cement, S_{pb}^N (MPa)	400
Particle radius (mm)	0.4 to 1.3	Shear strength of the cement, S_{pb}^S (MPa)	900
Particle density, ρ_s (kg/m ³)	2650	The percentage of bonded contacts, λ (%)	30
		The radius multiplier, α	Randomly distributed between 0 and 1

Figures

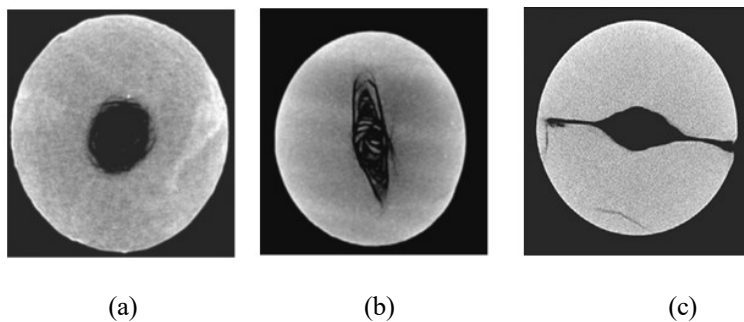


Fig. 1. Failure patterns of the hole in hollow cylinder sand production tests: (a) uniform failure, (b) dog-ear breakouts, (c) fracture-type breakout (Lavrov et al., 2005)

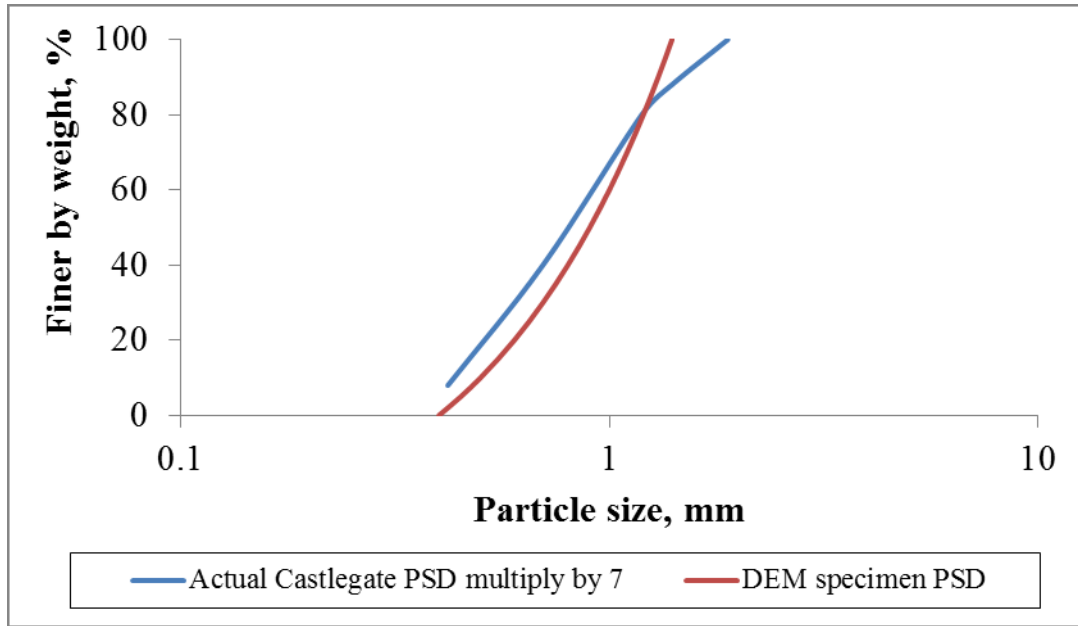


Fig. 2. Comparison between the actual Castlegate PSD and the DEM specimen PSD

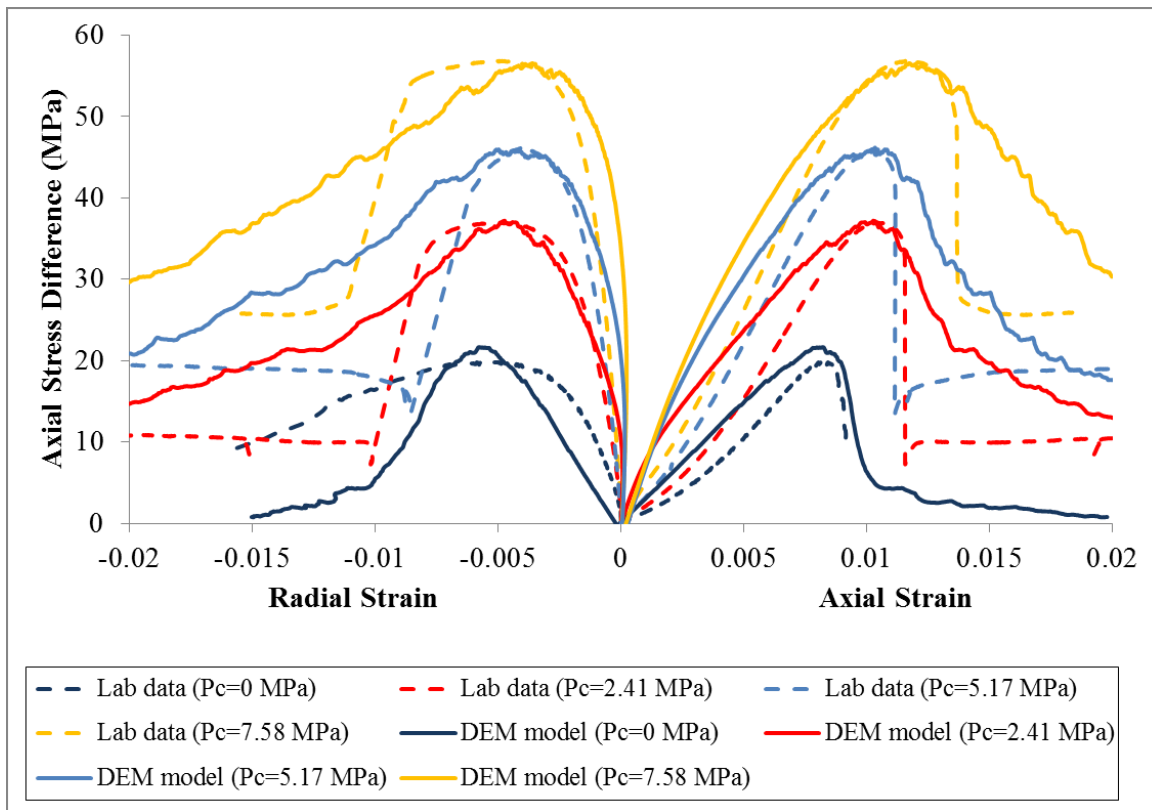


Fig. 3. Comparison between triaxial DEM model and laboratory results

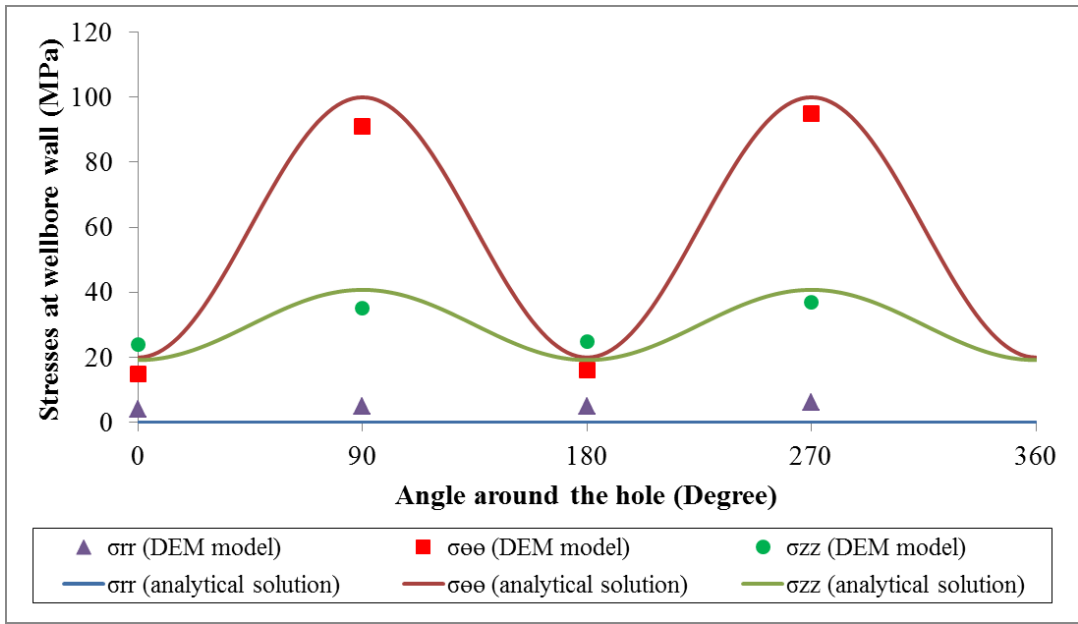


Fig. 4. Comparison of the stresses at the wellbore wall between the DEM model and the analytical solution developed by Zoback (2007)

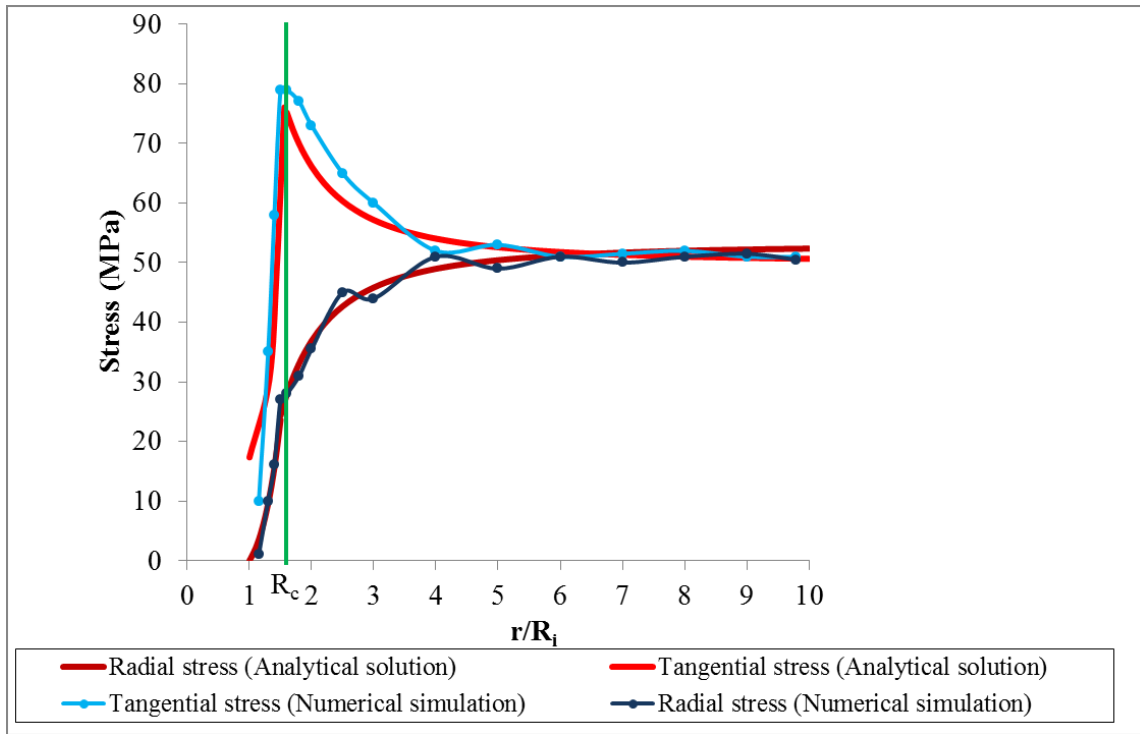


Fig. 5. Comparison of the stresses around the wellbore between the DEM model and the analytical solution developed by Risnes et al. (1982)

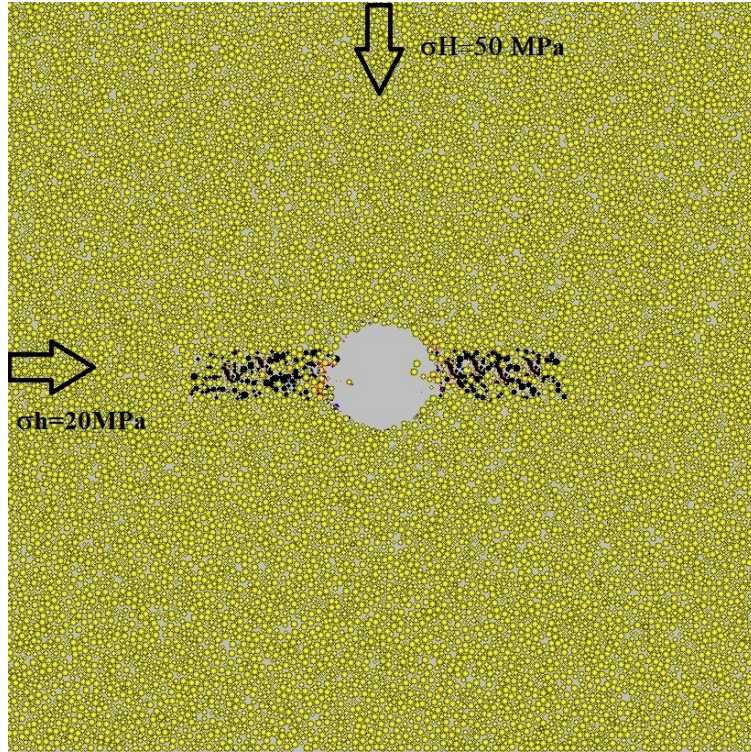


Fig. 6. Borehole cross-section of Castlegate sandstone showing fracture-like breakout ($\sigma_v=30$ MPa)

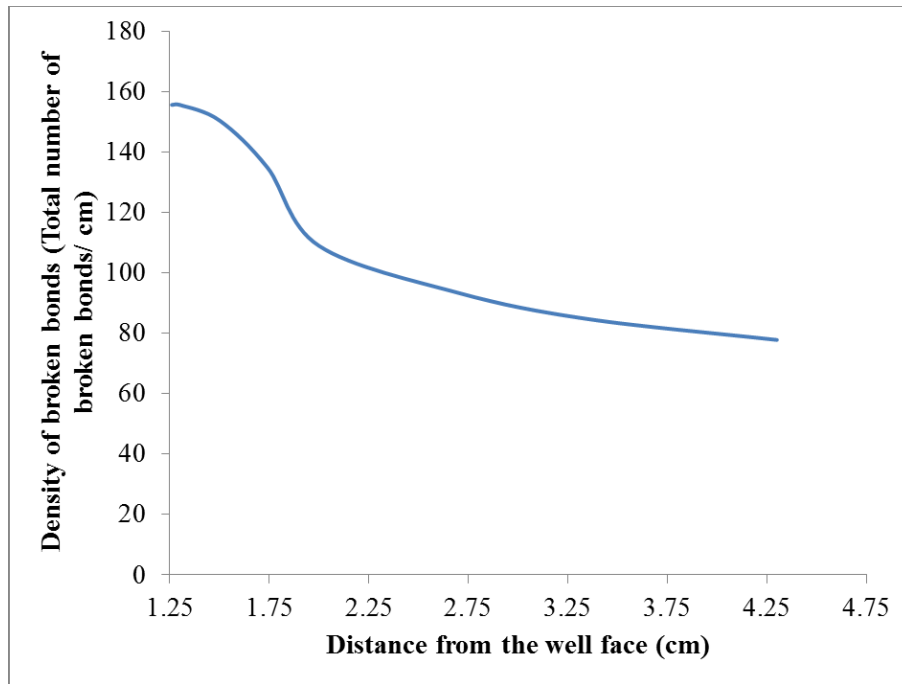


Fig. 7. Density of broken bonds within the compaction band ($\sigma_h=20$ MPa, $\sigma_v=30$ MPa, $\sigma_H=50$ MPa)

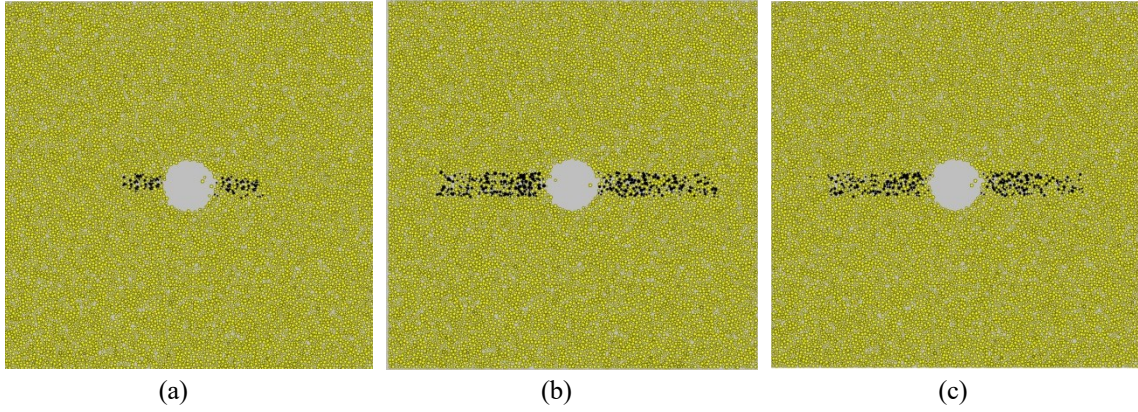


Fig. 8. borehole cross section of Castlegate sandstone at different far-field stresses (a) $\sigma_h=20$ MPa, $\sigma_v=30$ MPa, $\sigma_H=45$ MPa (b) $\sigma_h=20$ MPa, $\sigma_v=30$ MPa, $\sigma_H=60$ MPa (c) $\sigma_h=30$ MPa, $\sigma_v=35$ MPa, $\sigma_H=50$ MPa

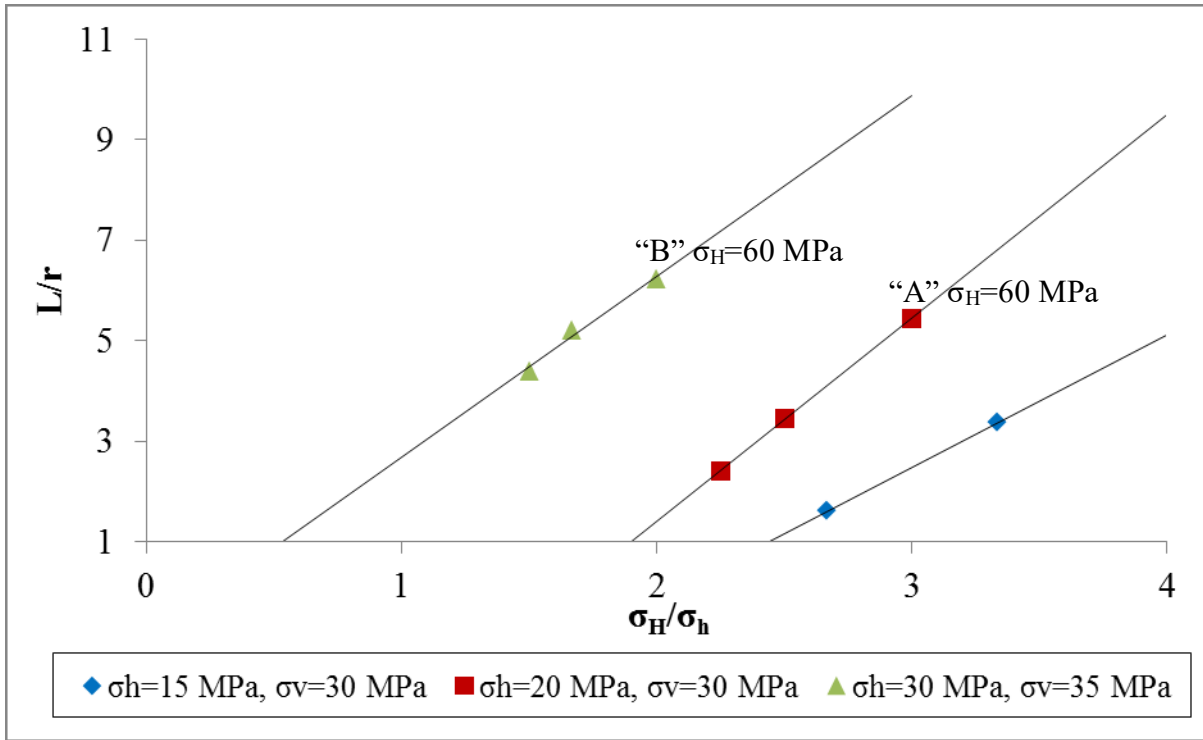
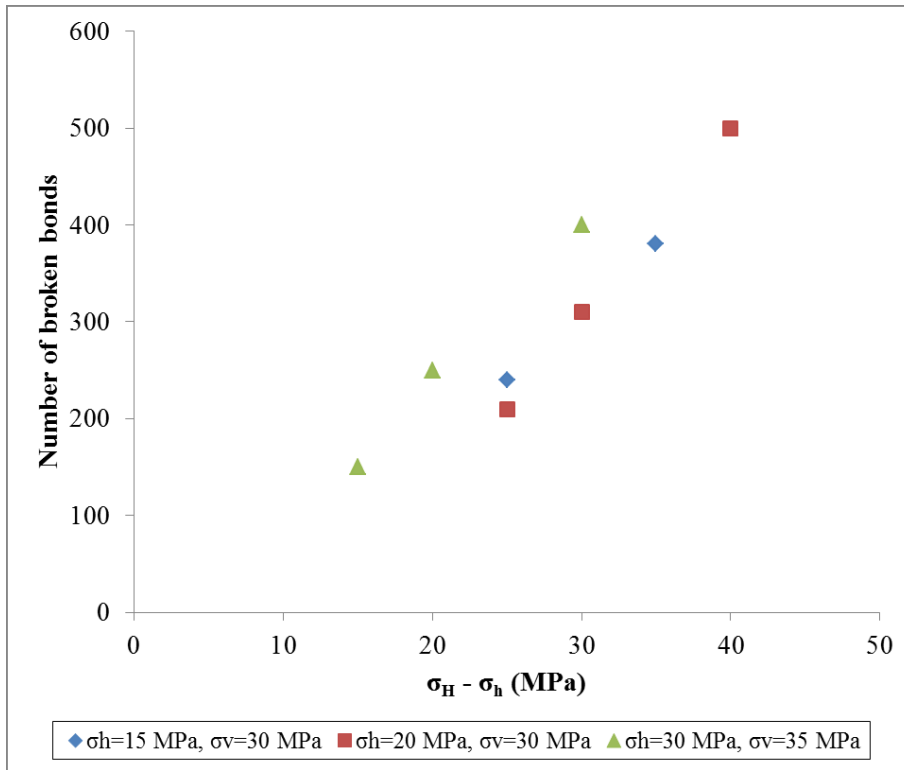
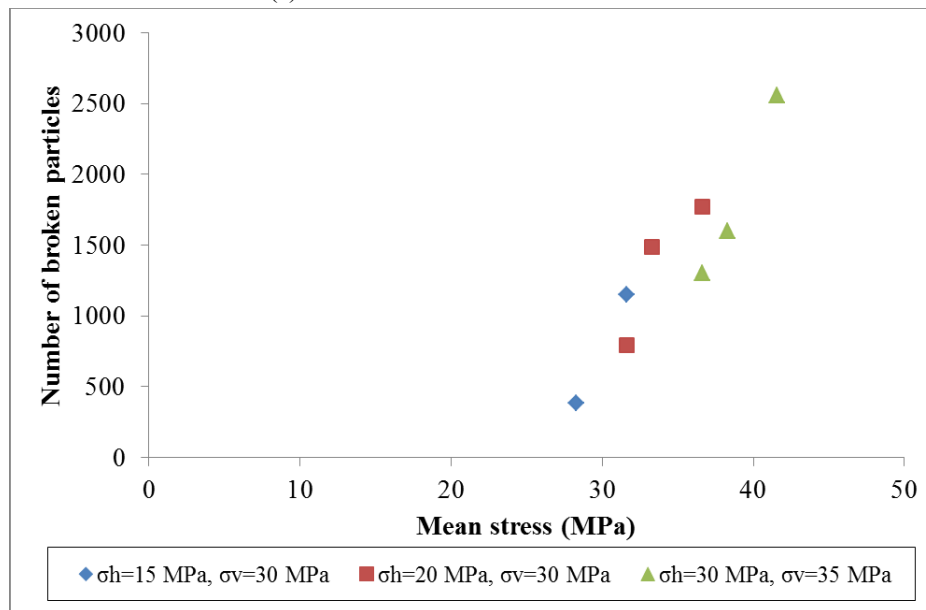


Fig. 9. Variation of normalized breakout length (L/r) in Castlegate sandstone as a function of σ_H/σ_h



(a) Total number of micro cracks



(b) Total number of broken particles

Fig. 10. Variation of micro cracks and crushed grains as function of mean stress and stress anisotropy